Title : Remote Sensing of Water Quality in an Australian Tropical Freshwater Impoundment using Matrix Inversion and MERIS Images.

Authors: Glenn Campbell[a,b,*] , Stuart R. Phinn[a], Arnold G. Dekker[c] and Vittorio E. Brando[c]

Affilliations: [a] University of Queensland, Centre for Spatial Environmental Research, School of Geography, Planning and Environmental Management, St Lucia, Queensland, Australia 4072

[b]University of Southern Queensland, Australian Centre for Sustainable Catchments & Faculty of Engineering and Surveying, Toowoomba Queensland, Australia 4350

[c]CSIRO Land and Water, Environmental Earth Observation Programme, Canberra, Australian Capital Territory, Australia 2601

[*]Corresponding author: Email: campbelg@usq,edu.au Ph: +61 7 4631 2909
Fax: +61 7 4631 2526
Postal Address: Faculty of Engineering and Surveying, University of Southern Queensland, West St, Toowoomba, Queensland, Australia 4350

Abstract

The purpose of this study was to investigate how semi-analytical inversion techniques developed for the remote sensing of water quality parameters (chlorophyll *a*, tripton and coloured dissolved organic matter (CDOM)) in inland waters could be adapted or improved for application to Australian tropical and sub-tropical water bodies. The Matrix Inversion Method (MIM) with a semi-analytic model of the anisotropy of the in-water light field was applied to MERIS images of Burdekin Falls Dam, Australia, a tropical freshwater impoundment. Specific attention was required to improve the atmospheric correction of the MERIS data. The performance of the conventional three band exact solution of the MIM was compared to that of over-determined solutions that used constant and differential weighting for each sensor band.

The results of the application of the MIM algorithm showed that the best weighting scheme had a mean chlorophyll *a* retrieval difference of 1.0 μgl^{-1}, the three band direct matrix inversion scheme had a mean difference of 4.2 μgl^{-1} and the constant weight scheme had a mean difference of 5.5 μgl^{-1}. For tripton, the best performed weighting scheme had a mean difference of 1.2 mgl^{-1}, the three band scheme had a mean difference of 3.4 mgl^{-1} and the constant weight scheme had a mean difference of 1.8 mgl^{-1}. For the CDOM retrieval, the mean difference was found to be 0.12 m^{-1} for the best performed weighting scheme, 0.25 m^{-1} for the three band scheme and 0.52 m^{-1} for the constant weight scheme. It was found that significant improvements in the accuracy and precision of retrieved water quality parameter values can be obtained by using differentially weighted, over-determined systems of equations, rather than exact solutions. These more reliable estimates of water quality parameters will allow water resource managers to improve their monitoring regimes.

1. Introduction

Water resource managers have the responsibility to deliver water of sufficient quality to urban, agricultural and industrial users as well as maintaining the recreational and ecological amenity of the inland water bodies under their control. To deliver these objectives it is critical that they understand and maintain the quality of the water in their storage reservoirs. Two of the important qualities of water that are relevant for the manager's objectives are turbidity of, and the level of algal activity within, the water body. The turbidity of the water, which is a major influence on the ecology of aquatic systems, is determined by the light absorption and light scattering processes that take place within the water column. Three water constituents (algal cells, suspended solids, and coloured dissolved organic matter (CDOM)) are major absorption and scattering agents within the water.

This research focuses on the semi-analytical approach to the optical remote sensing of water quality which is based on modelling the interaction of the light field with the optical properties of the water. The approach is not totally analytical as it uses empiricism to parameterise several of the terms in the model (O'Reilly et al. 1998; Rijkeboer et al. 1997). The physics based semi-analytical algorithms have the advantage of requiring less field data and allowing greater scope for multi-temporal series, which do not need repeated *in situ* measurements, to be developed.

Within the semi-analytical algorithms there are three general types; the look up table (LUT) approach which matches measured spectra to large number of previously calculated spectra (Keller 2001a; Matarrese et al. 2004; Mobley et al. 2005); the neural network (NN) approach which uses a large set of training data to relate the measured spectra to the parameters used to create the training set (Baruah et al. 2001; Doerffer and Schiller 2007; Schaale et al. 1998; Su et al. 2006); and the inversion / optimisation algorithms (Lee et al. 2002; Maritorena et al. 2002; Santini et al. 2010). In the inversion / optimisation approach a forward model is used to simulate the spectra from a number of parameters and the set of parameters that minimises a selected cost function are selected as the solution. If the forward model is linear and the cost function is the sum of the

squares of the residuals then this reduces to the linear matrix inversion method (Hoge and Lyon 1996). The first inland water study using this method, of the Dutch Lake Braassem, refers to it as the Matrix Inversion Method (MIM) (Hoogenboom et al. 1998b) and this term is used in this study.

A semi-analytical model estimates the measured reflectance as a function of the absorption and backscattering coefficients in each band and the MIM then solves the resultant system of linear equations. With the increase in the number of bands in more recent instruments there have been moves from using exact (same number of bands as unknowns) systems (Brando and Dekker 2003; Giardino et al. 2007; Hoge and Lyon 1996; Hoge et al. 1999; Hoogenboom et al. 1998b; Lyon and Hoge 2006) to over-determined (more bands than unknowns) systems (Boss and Roesler 2006; Hakvoort et al. 2002; Santini et al. 2010; Vos et al. 2003). Campbell and Phinn (2010) showed, through simulation, that significant improvements in the accuracy and precision of retrieved water quality constituent values can be obtained by using a differentially weighted over-determined system. The purpose of this work is to validate those results by applying the described methods to a tropical freshwater impoundment.

As 90% of the total radiance from a scene over a water body entering a sensor comes from the atmospheric path radiance (Vidot and Santer 2005) the accuracy of the atmospheric correction has a significant effect on the final accuracies of estimated water quality parameter concentrations. Some image based approaches for the atmospheric correction over case II waters for MERIS either simultaneously retrieve atmospheric and water components (Doerffer and Schiller 2008) or rely on the assumption that there is some quality of the water reflectance spectrum that is known or invariant (Moore et al. 1999). The focus for MERIS inland water remote sensing has been on temperate northern hemisphere environments and the inherent assumptions in the methods will not necessarily be appropriate for tropical and sub-tropical water bodies like Burdekin Falls Dam. Before the inversion algorithm could be applied to the image an atmospheric correction appropriate for the water body needed to be devised.

2. Data and Methods

In October 2008, fieldwork was conducted at Burdekin Falls Dam in northern Australia to parameterise the model using the methods described in Campbell and Phinn (2010). Whilst it is possible to make a rudimentary validation using the same measurements for the parameterisation and the validation, ideally the validation measurements should be independent of those used to parameterise the algorithm. To counter this problem another field campaign to Burdekin Falls Dam was mounted in August 2009 to obtain an independent validation set.

2.1 Site Description

The Burdekin Falls Dam (Lake Dalrymple, 20° 37´ S, 147° 0´ E) (Figure 1) is situated in the dry tropics region of Northern Australia. It receives inputs from four major sub-catchments that cover a total area of 114,000 km^2 and receive 70% of their rainfall in the December – March period of the year (Commonwealth Bureau of Meteorology 2010). From the north, the Burdekin River has its origin in tropical rainforest but primarily flows through tropical savannah. From the west, the lake is fed from the Cape River which rises in reasonably steep sedimentary country and then flows through flat less erodible areas. The Belyando and Suttor Rivers meet just beyond the inundated area and feed the lake from the south. The Belyando and Suttor Rivers suffer from persistent turbidity as they flow slowly over clay soils (O'Reagain et al. 2005). During full flow conditions the former river takes on a grey colour and the latter red. The highly variable particle size distributions that have been measured over single flow events in all tributaries (Lewis et al. 2009) suggest that the optical properties of the suspended sediment may be variable. It is estimated that the dam traps 88% of the sediment that flows in from the tributaries during flow events with the bulk of sediment being transported by the Burdekin River (Bainbridge et al. 2006a; Bainbridge et al. 2006b). However the majority of the turbidity in the water during no flow conditions is associated with the fine clays that are transported from the south (O'Reagain et al. 2005). The impoundment is split into an upper and lower basin by a narrow neck of land situated between measurement stations BFD9 and BFD11 shown in Figure 1.

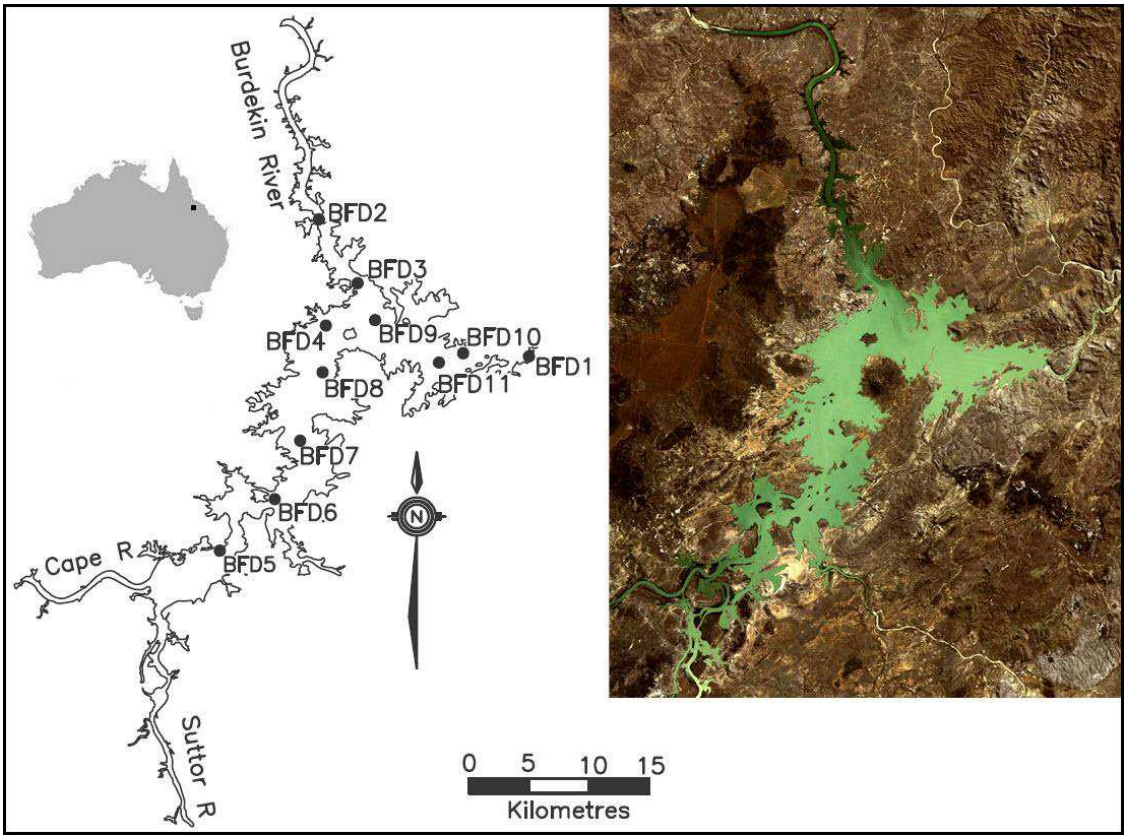

Figure 1 Location of the specific inherent optical property (SIOP) sample sites for the October 2008 fieldwork activities on Burdekin Falls Dam, Australia. The left hand image shows the calculated full supply level and the right hand image shows a Landsat 5 TM true colour image at the same scale as the map, captured on 22nd August 2008.

2.2 Water Quality Constituent Inherent Optical Property Models

The inherent optical properties (IOPs) of the water are modelled as a sum of the inherent optical properties of pure water and the water quality constituents suspended and dissolved in it.

2.2.1 Absorption

A four part absorption model was used.

$$a(\lambda) = a_w(\lambda) + a_{CDOM}(\lambda) + a_{TR}(\lambda) + a_\phi(\lambda) \quad (1)$$

The subscripts *w, TR* and ϕ refer to water, tripton (the non-algal particles of the suspended particulate matter) and chlorophyll *a* respectively. The values for $a_w(\lambda)$ were obtained from Pope and Fry (1997) and Smith and Baker (1981). The absorption due to

the water quality constituents is proportional to the concentration of the constituent. This is normally represented by the use of a specific absorption coefficient.

$$a_i(\lambda) = C_i a_i^*(\lambda) \quad (2)$$

The specific absorption spectra were sourced from the field measurements described below and are shown in Figure 4 (Campbell et al. 2011).

2.2.2 Scattering and Backscattering

The scattering coefficient *b* is combined with the volume scattering function (VSF) $\beta(\theta)$ to calculate the probability of a photon being scattered in a direction greater than 90°from its initial direction of travel. This is referred to as the backscattering.

A three part backscattering model was used.

$$b_b(\lambda) = b_{bw}(\lambda) + b_{bTR}(\lambda) + b_{b\phi}(\lambda) \quad (3)$$

The scattering coefficient for pure water was obtained from Morel (1974) and a ratio of b_w:b_{bw} of 0.5 was used. The backscattering of tripton and phytoplankton proportional to the concentration of the constituent were obtained from the field measurements described below and are shown in Figure 4 (Campbell et al. 2011) .

2.3 IOP and Water Quality Parameter Concentration Measurements

In situ water quality parameter measurements and near coincident MERIS images were obtained as part of two field campaigns. A summary of the methods used is given in Table 1.

Table 1 Dates of *in situ* and image data acquisition and a description of the laboratory methods used. The laboratory that performed the measurements is shown bracketed.

Fieldwork dates	Image Date	Chlorophyll *a* Concentration	Tripton Concentration	CDOM Concentration
13-15 Oct 2008	15 Oct 2008	HPLC (CSIRO)	Gravimetric (CSIRO)	Spectrophotometric (CSIRO)
12 August 2009	13 August 2009	US EPA 445.0 (AIMS)	n.d.	n.d.

2.3.1 Laboratory Measurements

October 2008 Measurements

During October 2008 the IOPs of the storage were measured at eleven stations (see Figure 1). Water samples were taken from approximately 0.3 m below the surface and kept cool for later laboratory measurement of tripton (TR), chlorophyll *a* (CHL) concentration and coloured dissolved organic matter (CDOM) absorption at 440 nm and spectral absorption.

The chlorophyll *a* concentration was measured with HPLC following a modified version of the Van Heukelem and Thomas (2001) method. The tripton water samples were filtered through pre-weighed Whatman GF/F glass-fibre filters that had been prepared according to the MERIS calibration protocols (Tilstone et al. 2002) and oven-dried at 60ºC to constant weight and weighed. The algal and non-algal spectral absorption was measured over the 200-900 nm spectral range in 1.3 nm increments, using a GBC 916 UV/VIS dual beam spectrophotometer equipped with an integrating sphere. The pigmented material on the sample filter was then extracted using the Kishino et al. (1985) method and then the filter was remeasured to determine the optical density of the non-algal particles. CDOM samples were collected in glass bottles and filtered through a 0.22 µm polycarbonate filter (Millipore) using an all glass filtering unit and absorbance was measured from 200 to 900 nm using a 10 cm path length quartz cell with Milli-Q water (Millipore) as a reference. The scattering properties were measured *in situ* using a HydroScat-6 backscattering sensor (Maffione and Dana 1997). A detailed description of the IOP measurements, water quality parameter measurements and subsequent specific inherent optical property (SIOP) domain calculation is provided in Campbell et al. (2011).

August 2009 Measurements

A second field campaign was conducted in August 2009 to obtain a larger validation dataset that was independent of the measurements used to parameterise the algorithm.

Water samples were taken from approximately 0.3 m below the surface at 25 observations stations (shown in Figure 2). As the concentration of CDOM is not of interest to Australian water managers it was decided that it was preferable to allocate the available resources to building a more extensive validation set for the chlorophyll *a* and tripton products. Unfortunately inadequate laboratory procedures prevented the determination of the tripton concentrations for the 2009 campaign.

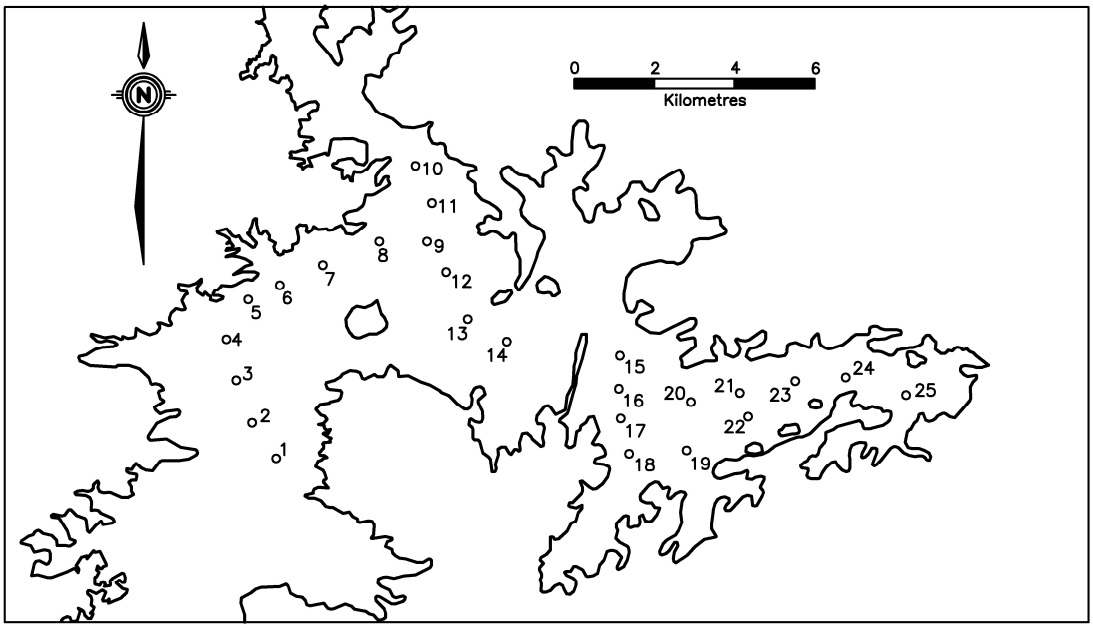

Figure 2 Location of the 25 validation sample sites for the August 2009 fieldwork activities on Burdekin Falls Dam, Australia.

During the second campaign the water samples taken at each station were kept cool in opaque storage containers and were filtered on the day of collection.

Phytoplankton Pigments

Two replicates were prepared for each water sample by filtering through a 47 mm diameter GF/F glass-fibre filter (Whatman, nominal pore size; 0.7 μm) and then freezing the filter.

The pigments were measured using the US EPA method 445.0 (Arar and Collins 1997). This method measures the combined concentrations of chlorophyll *a* and pheophytin *a.* With the aid of HPLC analysis no pheophytin *a* was detected in the October 2008

samples so it is assumed that the measured concentration is only that of chlorophyll *a*. The pigments were extracted from the phytoplankton in 90% acetone and then centrifuged to clarify the solution. The solution was transferred to a glass cuvette and the chlorophyll fluorescence was measured before and after acidification to 0.003 N HCl with 0.1 N HCl.

To get an indication of the repeatability of the measurement method, replicates, for each measurement station were, created by first dividing the water sample in two before filtering each half onto separate filters. Figure 3 compares the measured chlorophyll *a* concentrations for each replicate. The differences between the replicates had a mean of 0.3 μgl^{-1} (8%) and a standard deviation of 0.35μgl^{-1} (9%) and the maximum difference was 1.36 μgl^{-1} (33%).

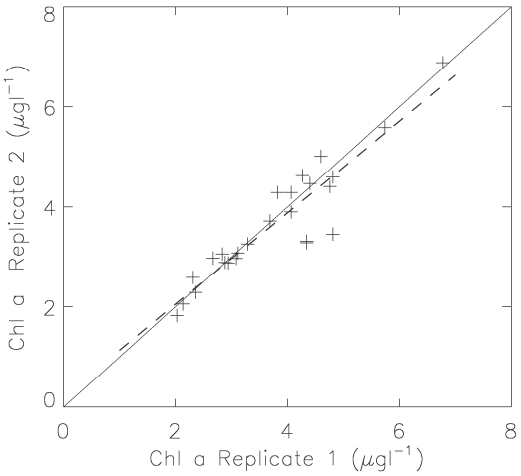

Figure 3 Plot comparing the measured chlorophyll *a* concentrations for the two replicates of each measurement station for the 12th August 2009 Burdekin Falls Dam fieldwork. The dashed line is the line of best fit which has a slope of 0.916, an intercept of 0.22 μgl^{-1} and an R^2 of 0.855. The solid line is the line of 1:1 correspondence.

2.3.2 SIOP Domains

Notable intra-impoundment variation in the specific absorption and specific scattering of phytoplankton and tripton was found among the stations measured during the 2008 fieldwork activities. As a result, the water in Burdekin Falls Dam was characterised by

two SIOP sets, the upper basin and the lower basin that are shown in Figure 4 (Campbell et al. 2011).

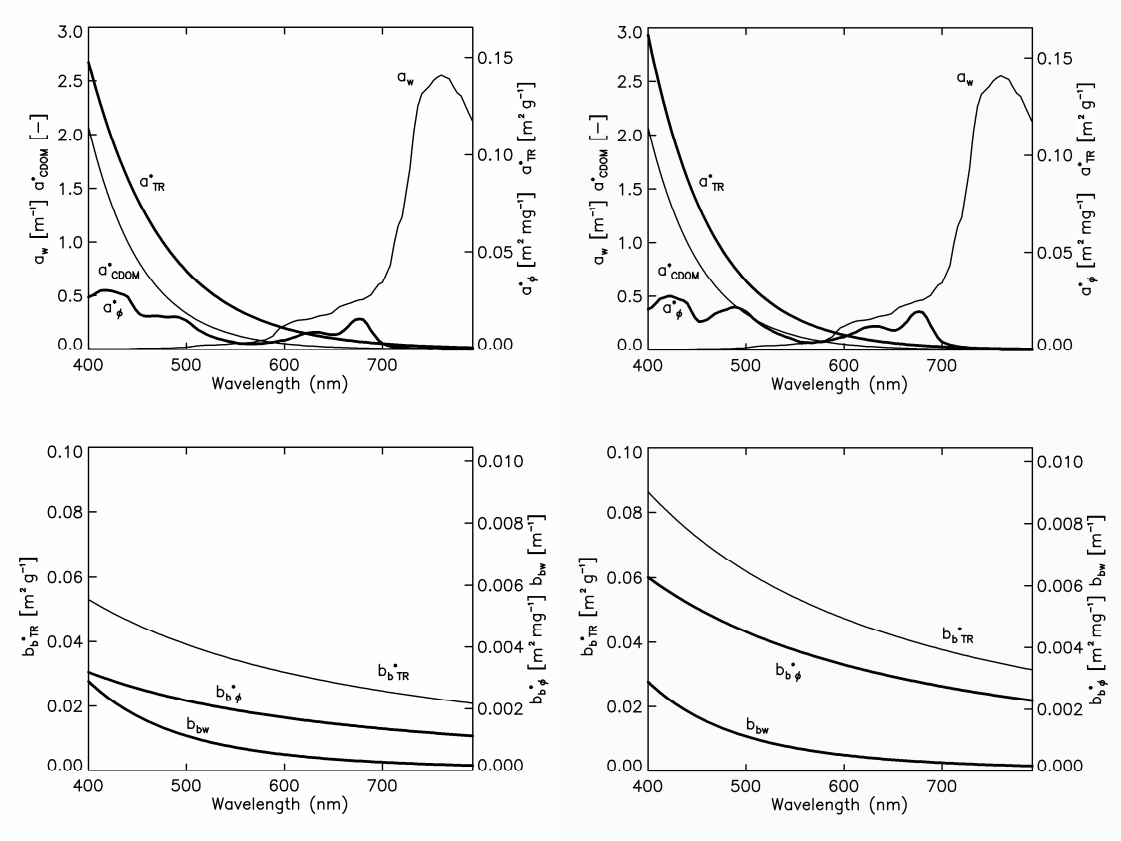

Figure 4 SIOP sets upper basin (left) and lower basin (right) for Burdekin Falls Dam measured during the October 2008 field work. The upper graph shows the spectral absorption of water (*w*) and the chlorophyll *a* specific absorption spectra of phytoplankton (ϕ), tripton (*TR*) and coloured dissolved organic matter (*CDOM*). The lower shows the spectral backscattering of water (*w*) and the specific backscattering spectra of chlorophyll *a*(ϕ) and tripton (*TR*).

The primary distinction between the two SIOP domains is the higher tripton specific backscattering found in the lower basin SIOP set.

2.4 In Situ Spectroradiometric Data

Two RAMSES spectroradiometers were mounted in a cage. One spectroradiometer was fitted with a cosine collector and was orientated in the cage to measure the downwelling irradiance (E_d) and one radiance collector was orientated to measure the upwelling radiance (L_u). The cage was lowered on the unshaded side of the vessel to minimize the shading effects. For each station of the 2008 field campaign, simultaneous measurements

of E_d and upwelling radiance L_u were combined to calculate the above surface reflectance. Observations for stations 9-11 are used throughout this paper for comparison as they were made within ninety minutes of the acquisition of the 15th October 2008 MERIS image.

2.5 Image Processing Chain

To create the final water quality parameter map, the level 1b full resolution MERIS image (see Table 1) was first corrected to remove the influence of the air-water interface and atmosphere and processed to produce a subsurface irradiance reflectance image of the water. For each weighting scheme the MIM inversion was then applied using both SIOP sets in turn, to produce two water quality images corresponding to each of the SIOP domains. For each pixel in the image the optimal SIOP set was identified and the corresponding retrieved concentrations were combined to create the final water quality parameter image.

2.6 Atmospheric Correction

It would have been possible to correct the October 15th 2008 image by using the collected *in situ* spectroradiometric observations that were coincident with the satellite overpass (Stations 9-11). The collection of *in situ* spectroradiometric observations is both time consuming and expensive, so any long term or archival monitoring project needs to come to terms with how the images can be corrected in the absence of *in situ* data. One approach is to take advantage of the homogeneity of aerosols over small spatial scales of 50-100 kms (Vidot and Santer 2005) to calculate the correction parameters and then apply them to the water body. A simplified version of this approach was used where the aerosol model was pre-selected rather than estimated from the image. The correction was applied to both images and was evaluated by comparing the corrected 2008 image to the *in situ* spectroradiometric observations at Stations 9-11.

The c-WOMBAT-c software (Brando and Dekker 2003) implements an established theoretical framework using atmospheric parameters generated by multiple runs of the radiative transfer code MODTRAN-4 (Adler-Golden et al. 1998; de Haan et al. 1999). In

this study the c-WOMBAT-c code was modified to use the 6S radiative transfer code as an extensive test between 6S, MODTRAN, RT3 and SHARM radiative transfer codes (Kotchenova et al. 2008) found that 6S was the most reliable code for calculation of solar radiation reflected and transmitted by a plane-parallel, non-absorbing molecular atmosphere. In addition, the relatively fast scalar option within MODTRAN-4 does not account for the azimuthal dependence of the multi-scattering solar contribution (Acharya et al. 1999). To take this into account the user must select the more accurate but much slower DISORT N-stream method which limits its practicality for multiple runs at multiple aerosol optical thicknesses.

The 6S code requires the user to specify a number of geometric and aerosol characteristics. The aerosol optical thickness (AOT) at 550 nm parameter is the most significant and quickly varying parameter. *In situ* spectroradiometric observations were taken at stations 9-11 on the same morning as the satellite overpass. The AOT value was tuned to minimise the sum of the differences between corrected spectra and these *in situ* overpass stations. To make allowance for image noise and geo-referencing uncertainty the image spectra for each station were taken to be the average spectra from the four pixels that are closest to the co-ordinates for the *in situ* measurement.

The atmospherically corrected Burdekin Falls Dam MERIS water pixels were compared with the *in situ* spectroradiometric observations taken at stations 9-11 (Figure 5). There was a significant anomaly below 500 nm which appears in spectra corrected with the de Haan et al. (1999) formulation in other published work (Bagheri et al. 2005; Candiani et al. 2007a; Sterckx and Debruyn 2004). The MERIS instrument performs a calibration every two weeks using diffuser plates illuminated by the Sun. The absolute radiometric gains are calculated by comparing the averaged signal to the on-ground characterisation of the diffuser (ESA 2006). The MERIS sensor is calibrated using the Thuillier et al. (2003) reference sun irradiance spectrum as recommended by the Committee on Earth Observation Satellites (CEOS) (CEOS 2008). This model was compared to the default MODTRAN-4 solar illumination database and a major difference was found around 440 nm (see Figure 5 a)). As the sensor gains are calculated with

reference to this model the same model must be used to calculate the reflectance spectrum. Figure 5 b) and c) shows that when the correction was re-run using the new reference sun the anomaly was eliminated.

Adjacency effects occur when atmospheric multiple scattering makes photons reflected from the area around the target pixel appear to be originating from the target pixel. This is particularly pronounced when the target pixel is much darker than the surrounding area and the aerosol loading in the atmosphere is high. Due to the size and shape of the target water bodies and inland waters in general, a substantial proportion of pixels can be contaminated by the adjacency effect. Keller (2001b) conducted an experiment to evaluate the theoretically expected adjacency effect, but found no significant contribution. In contrast, Candiani et al. (2007b) found the steep forested hills that border the northern section of the Lake Garda in Italy, contributed a noticeable contamination of the water spectra and Vos et al. (2003) eliminated all pixels within 1 km of the shoreline as they found that spectra were too corrupted for an accurate retrieval of the water quality parameter concentrations. The gentle topography and low aerosol loading that typifies the study site is likely to keep any adjacency effect to a minimum. The c-WOMBAT-c approach to correcting for the adjacency effect applies an *n x n* low pass filter to the image to supply the average radiance ($L_{rs,b}$) image. The implicit assumption is that every part of that area contributes the same to the environmental radiance. The size of *n* has previously been nominated as a figure that produces the appropriate amount of adjacency effect. However, the effect of the background reflectance (ρ_b) is more complicated and can be represented by the integration of small contributions over the background area (Vermote et al. 2006). The spatially averaged background reflectance for a point *M* is

$$\langle \rho_b(M) \rangle = \frac{1}{t_d(\theta_v)} \int_{-\infty}^{\infty} \int_{-\infty}^{\infty} \rho'(x, y)\, e(x, y, \theta_v)\, dx\, dy \qquad (4)$$

where ρ' is the reflectance of a small section of the background at coordinates of (x,y) from the centre of the target and t_d is the diffuse transmittance. The function *e* is the contribution to the diffuse transmittance from that position (x,y). This expression can be

converted to deal with polar co-ordinates of near vertical observation (θ_v <30°). If the background reflectance is assumed homogenous a division can be made between the target of radius *r* and the background. The fraction of the diffuse transmittance that the target is responsible for becomes:

$$F(r) = 2\pi \int_0^r e(r, \phi, \theta_v) dr \tag{5}$$

This reasoning can be applied to model the average background radiance as $\langle L_b(M) \rangle = L_c F(r) + (1 - F(r)) L_b$ where L_c is the image and L_b is an *n x n* pixel low pass filter. Vermote et al. (2006) evaluate the *F(r)* for a particular *e*. Using diffuse transmittance calculated with 6S showed that *F(r)* had a small spectral dependence with a maximum in the blue part of the spectrum and a minimum in the NIR part. For *r* = 0.15km (for MERIS) an average value of *F(r)* = 0.118 was used.

An understanding of the scale of the adjacency effect was obtained by running the modified c-WOMBAT-c algorithm using background images described above with values of *n* from 3 to 15 and comparing it to a run which uses the image itself as a background file. By comparing *in situ* spectra that were co-incident with the satellite overpass with the image processed with alternative values of *n* it should be theoretically possible to nominate an optimal value for *n*. However, the standard deviation of the *in situ* observations in the case of Stations 10 and 11 was larger than the range of the calculated adjacency effect (see Figure 6). Relying solely on Station 9, a value of *n* = 9 was found to minimise the sum of the differences between image and *in situ* spectrum. This value results in a 2.7 km x 2.7 km adjacency window.

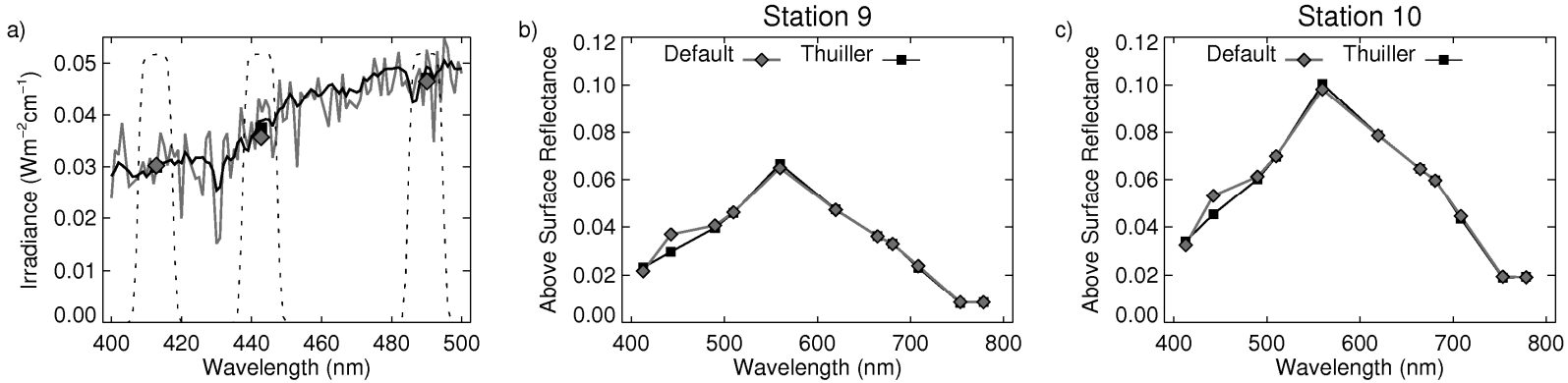

Figure 5 Comparison of two MODTRAN solar irradiance databases. a) The default MODTRAN database (newkur.dat) is shown in grey and the Thuiller database (thurkur.dat) is shown in black. The databases were convolved with the MERIS band response function (shown dotted) to produce estimated values for the default database shown by diamonds and the Thuiller database depicted by squares. b) an d c) Mean above surface reflectance spectra of the corrected Burdekin Falls Dam water pixels at Stations 9 and 10. The image was corrected using the MODTRAN-4 two stream model and the Thuillier et al (2003) and the MODTRAN-4 default reference sun irradiance. No correction for the adjacency effect has been made.

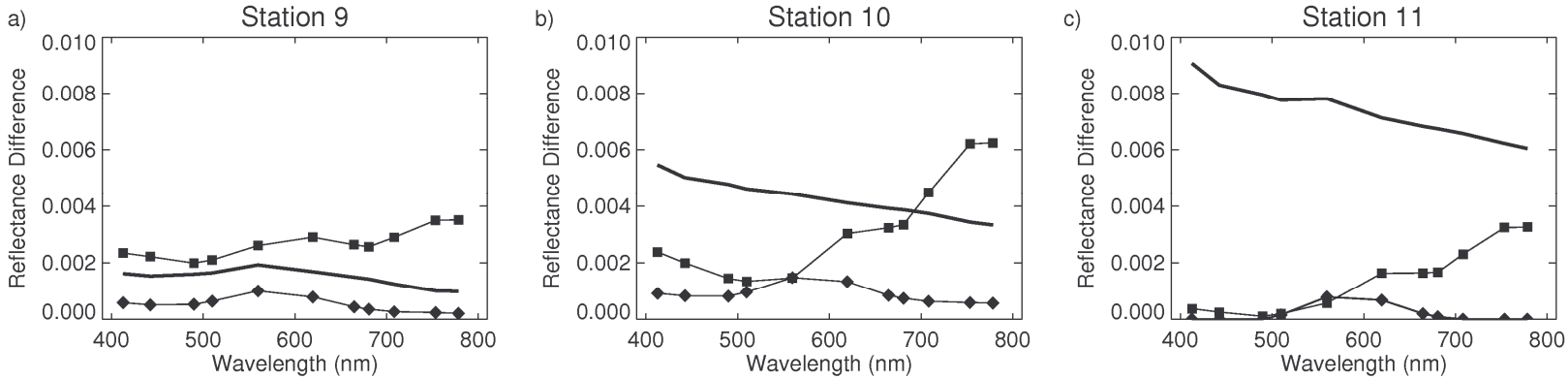

Figure 6 The amount of correction for the adjacency effect for a 3 x 3 (diamonds) and a 15 x15 (squares) adjacency window, a) Station 9, b) Station 10 and c) Station 11. The thick line shows the standard deviation in the *in situ* observations.

The Vidot and Santer approach assumes that the reflectance value of the dense dark vegetation (DDV) in the blue and red regions is known and uses these values to identify the aerosol type and retrieve the aerosol optical thickness. In this work the aerosol type was selected based on the water body location and the prevailing wind conditions prior to the image acquisition. The reference DDV values for three bands (412, 443 and 665 nm), corrected for the BRDF effects using the Leroy et al. (1998) model, were extracted from the MERIS auxiliary files: model 9 *equatorial_asia_nov* for September – February and model 20 *equatorial_asia_june* for March – August. Image pixels were designated as DDV pixels if their Atmospherically Resistant Vegetation Index (ARVI) (Kaufman and Tanre 1992) was above a given threshold. The ARVI was calculated by

$$ARVI = \frac{\rho_{aG}^{NIR} - \rho_{aG}^{rb}}{\rho_{aG}^{NIR} + \rho_{aG}^{rb}} \tag{6}$$

$$\rho_{aG}^{rb} = \rho_{aG}^{r} - \gamma\left(\rho_{aG}^{b} - \rho_{aG}^{r}\right) \tag{7}$$

where ρ_{aG} is the remote sensing reflectance in the blue (*b)* (443 nm), red (*r*) (665 nm) and NIR (865 nm) bands that has been corrected for molecular scattering and gaseous absorption. This molecular scattering and gaseous absorption corrected image is created by running the c-WOMBAT-c code described above with an AOT of 0.0. The selection of γ is left to the discretion of the user. Santer et al. (2006) showed that the value of γ has little effect on the ARVI threshold for aerosols dominated by large particles and the value $\gamma = 1.3$ is the most robust in the case of small particle dominated aerosols. The value of $\gamma = 1.3$ was used (Floricioiu and Rott 2005; Santer et al. 1999; Vidot and Santer 2005). A simple ARVI threshold is prone to select normal vegetation that is shadowed by cloud at the time of the image acquisition. The reflectance value in the 865 nm band was used to separate cloud shadow from DDV using a minimum reflectance of 17% (Floricioiu and Rott 2005) and a subset of image pixels that represented the highest 0.5% of ARVI values was selected. The DDV pixel subset was averaged to get the DDV spectrum for that AOT

value. The AOT value was iterated until the image DDV value matched the reference DDV.

2.7 Matrix Inversion Method

A version of the Gordon et al. (1975) subsurface irradiance reflectance ($R(0^-)$) model, with the higher order terms neglected, was used:

$$R(0^-, \lambda_i) = f(\omega_b, \mu_0, \lambda_i) \frac{b_b(\lambda_i)}{a(\lambda_i) + b_b(\lambda_i)} \quad (8)$$

The proportionality factor (f) was modelled as a cubic function of the subsurface reflectance and the sun zenith angle calculated from Hydrolight ® simulations (Campbell and Phinn 2010). The absorption and backscattering models described in Equations 1-3 were substituted into Equation 8 (Brando and Dekker 2003). Rearranging the equation and putting it in matrix form for all wavelengths of the spectra leads to Equation 9 (Hoogenboom et al. 1998b).

$$\begin{bmatrix} a_w(\lambda_1)\frac{R(\lambda_1)}{f} - b_{bw}(\lambda_1)\left(1 - \frac{R(\lambda_1)}{f}\right) \\ \vdots \\ a_w(\lambda_n)\frac{R(\lambda_n)}{f} - b_{bw}(\lambda_n)\left(1 - \frac{R(\lambda_n)}{f}\right) \end{bmatrix} = \begin{bmatrix} a^*_\phi(\lambda_1)\frac{R(\lambda_1)}{f} - b^*_{b\phi}(\lambda_1)\left(1 - \frac{R(\lambda_1)}{f}\right) & \cdots \\ \vdots & \cdots \\ a^*_\phi(\lambda_1)\frac{R(\lambda_1)}{f} - b^*_{b\phi}(\lambda_1)\left(1 - \frac{R(\lambda_1)}{f}\right) & \cdots \end{bmatrix} \begin{bmatrix} CHL \\ TR \\ CDOM \end{bmatrix} \quad (9)$$

or

$$\mathbf{y} = \mathbf{Ax} \quad (10)$$

Where **A** is a 3 x N dimension matrix with N being the number of bands utilised by the inversion.

The solution of this equation uses a square (NxN) weight matrix which is a diagonal matrix (W) where W_{ii}= relative weight of band *i*. The solution then becomes

$$\mathbf{x} = \left[\mathbf{A}^T\mathbf{W}\mathbf{A}\right]^{-1}\mathbf{A}^T\mathbf{W}\mathbf{y} \quad (11)$$

2.8 Weighting Schemes

A large number of weighting schemes were investigated and seven are reported here. The first two schemes represent the conventional approach where all bands are given equal weighting (NO_WEIGHTS) or where exactly determined systems of equations of *a priori* selected bands are used (3BANDS). In this case the three bands selected were as close as possible to those used by Brando and Dekker (2003) for a turbid coastal embayment in a subtropical coastal area, two centred at 490 and 670 nm and one in the 700-740 nm range. The next scheme represents the assumption that that there is a uniform noise in reflectance (Hakvoort et al. 2002) meaning that those bands with a high value of reflectance should have a higher signal to noise ratio and thus will be more reliable (REF). Giardino et al. (2007) and Hoogenboom et al. (1998a) make the argument that bands which exhibit the greatest change in reflectance when an increase in a water quality constituent concentration occurs should be of greater use in determining the concentration. This assumption was represented by a scheme that weighted the bands by the first derivative of the simulated spectra with respect to the water quality constituent concentration (DER). The last two schemes were derived empirically (RAN). Inversions were run using the previously mentioned Hydrolight ® simulations as the subject spectra. The weights were allowed to vary randomly and those that returned the water quality parameters that were closest to the values used in the simulation were retained and the commonalities of the best performed schemes were combined. In addition to the unweighted inversion, a total 37 weighting schemes were trialled but only the results of a representative subset shown in Figure 7 will be reported.

2.9 SIOP Domain Selection

An image or inversion based measure that selected the optimal SIOP set was used. Phinn et al. (2005) used the difference between the imagery $R(0^-)$ and the 'inverse-forward' simulated $R(0^-)$ as a measure of the optical closure of each pixel. This approach was implemented by using the sum of the squares of the difference between the imagery $R(0^-)$ and the 'inverse-forward' simulated $R(0^-)$. For convenience this will be called the mis-close sum.

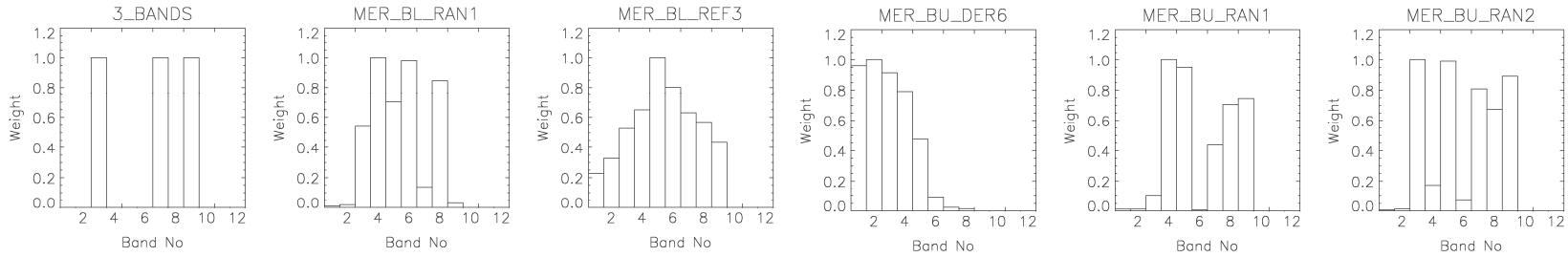

Figure 7 The weights for the selection of weighting schemes reported in the results sections. The band numbers relate to the MERIS sensor with nominal band centres of (1) 412.5 nm, (2) 442.5 nm, (3) 490 nm, (4) 510 nm, (5) 560 nm, (6) 620 nm, (7) 665 nm, (8) 681.25 nm, (9) 708.75 nm, (10) 753.75 nm, (11) 760.625 nm and (12) 778.75 nm.

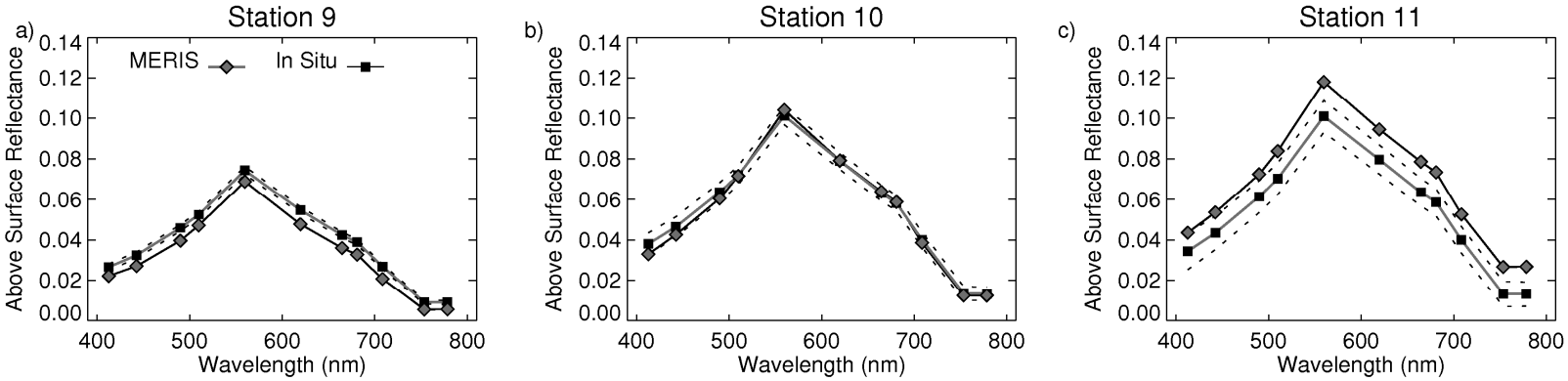

Figure 8 Comparing the *in situ* spectroradiometric measurements with the corrected image for 15th October 2008 at Burdekin Falls Dam. The diamonds show the mean spectra of four pixels closest to the *in situ* measurement and the black squares show the mean of the *in situ* spectra. The dotted lines represent one standard deviation either side of the mean for the *in situ* measurements. The observations were made within 1½ hours of the MERIS image of 15th October.

3. Results

3.1 Atmospheric Correction

The corrected October 15th 2008 image was compared to the *in situ* measurements for stations 9-11 and the comparison is shown in Figure 8 and the results were comparable to recent observations made at European lakes using the SCAPE-M (Guanter et al. 2010) and the BEAM Case-2 Regional atmospheric corrections (Odermatt et al. 2010). It should be noted that the direct comparison of *in situ* measurements and the image pixel is hampered by complications arising from the homogeneity of the water, the difference in the instantaneous field of view of the sensors and the inherent noise in the image. Even if it is assumed that the adjacency effect has been fully accounted for, the MERIS image pixel still represents an average spectrum for an area of 290 m x 260 m.

3.3 SIOP Selection

Selecting the SIOP set that corresponded to the lower of the two mis-close sums meant the lower basin SIOP set was selected for only 4.3% of the pixels and those were in the extreme upstream ends of the water storage. This was an unexpected result as SIOP measurements made at the time of the image acquisition (Stn 10 &11 – 15th October 2008) measured directly the SIOPs in the water and found them to be closer to the lower basin SIOP set.

To investigate the significance of the differences between the mis-close sums that result from using each of the two SIOP sets, the pixels were separated into upper basin and lower basin groups based on their geographic position. The comparison between the mis-close sums resulting from the two SIOP sets is displayed in Figure 9, which shows a clear trend for the ratio between the mis-close sums to be lower for the lower basin group of pixels. Lines of best fit were calculated for the two groups with gradient and R^2 values of 0.877 and 0.992 for the upper basin SIOP set and 0.818 and 0.986 for the lower basin SIOP set. In both cases the y intercept was negligible, so the ratio of the lower and upper mis-close sums was calculated and considered. The ratio of the upper basin SIOP set mis-close sums to the lower basin SIOP set mis-close sums was generally higher for

those pixels that represented water in the upper basin. The inversion was rerun and this time a threshold of 0.847 for the ratio of the mis-close sum was used to select the appropriate SIOP set.

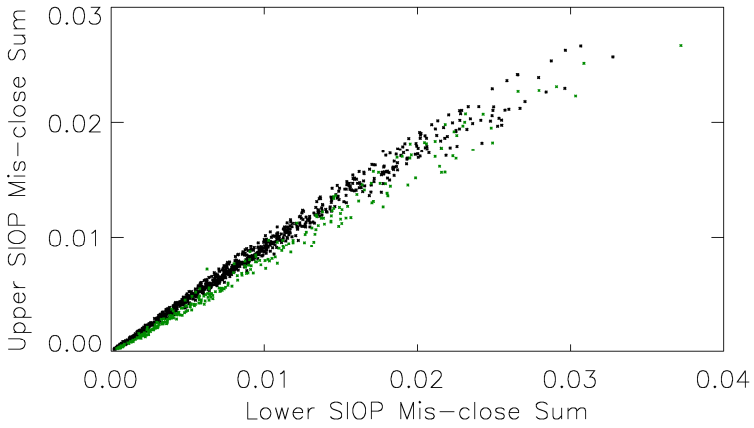

Figure 9 The mis-close sum that results from the lower basin SIOP set against the mis-close sum that results from using the upper basin SIOP set. Those data associated with pixels in the upper basin group are plotted in black and those associated with the lower basin group are plotted in green.

In this case the result is much more keeping with the SIOP measurements made at the time of the image acquisition. Aside from the lower area that was used to calculate the threshold, the method identified an area around the former confluence of the Burdekin and Suttor Rivers. The tripton specific backscattering spectrum that was measured in this area (Stn 4) showed the largest slope measured in the upper basin region, much closer to the lower basin than the other upper basin observations.

3.4 Water Quality Parameter Maps 15th October 2008

The water quality parameter maps produced from the 15th October 2008 image are shown in Figure 10 and a comparison of the laboratory concentrations and image retrieved concentrations for selected weighting schemes are shown in Figure 11. The *in situ* samples were taken in a 48 hr period prior to the satellite overpass. The means of the absolute values of difference between the laboratory measured concentrations and those retrieved from the image are shown in Table 2.

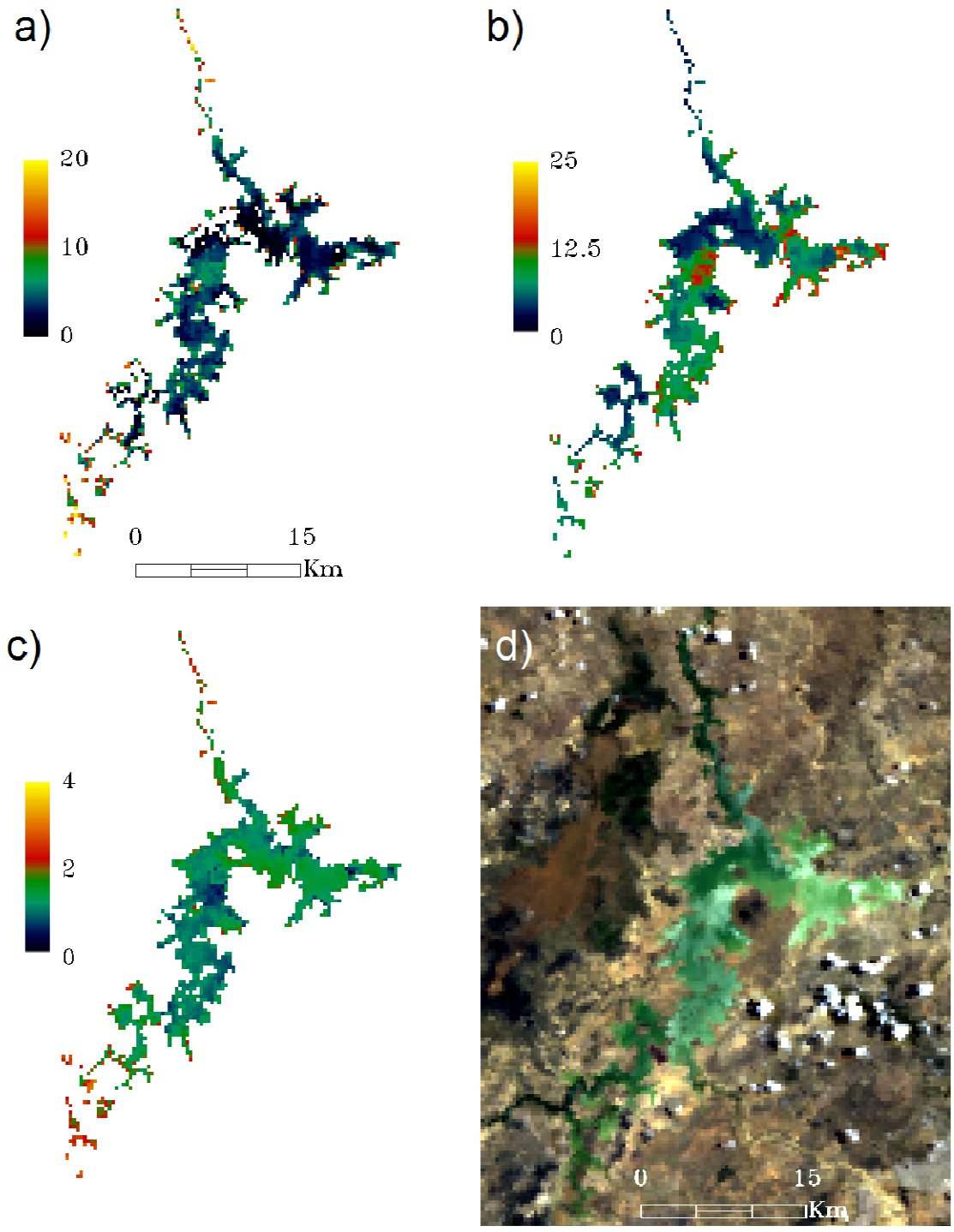

Figure 10 Maps of the water quality parameters retrieved from the 15th October 2008 image using the ratio threshold and the MER_BU_RAN2 weighting scheme. a) Chlorophyll *a*, b) Tripton, c) CDOM and d) True colour MERIS image. Approximately 5% of the pixels returned a physically impossible negative concentration for chlorophyll a. The pixels have been masked out of image a).

Table 2 The means of the absolute values of difference between the laboratory measured concentrations and those retrieved from the 15th October 2008 image and the ratio threshold for selected weighting schemes.

	Chl (μgl^{-1})		TR (mgl^{-1})		CDOM(m^{-1})	
	Av	SD	Av	SD	Av	SD
NO_WEIGHTS	4.31	2.82	1.79	1.23	0.52	0.26
3_BANDS	7.72	5.53	3.39	3.04	0.25	0.25
MER_BL_RAN1	13.8	5.35	1.74	0.84	0.12	0.11
MER_BL_REF3	3.88	3.31	1.24	1.07	0.39	0.24
MER_BU_DER6	3.28	2.16	4.22	1.12	0.87	0.18
MER_BU_RAN1	1.44	1.68	2.71	2.36	0.28	0.17
MER_BU_RAN2	1.66	1.62	2.69	2.35	0.25	0.18

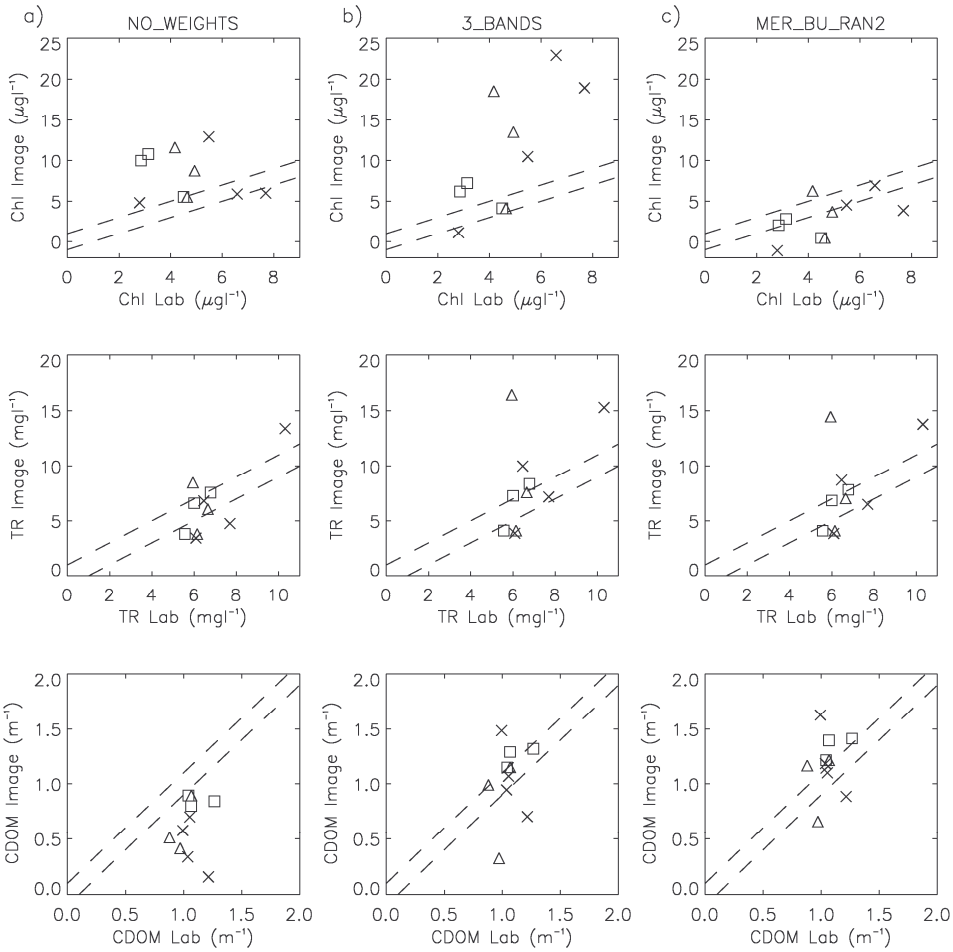

Figure 11 The laboratory concentrations vs. image retrieved concentrations for selected weighting schemes for the 15th October 2009 image, a) Unweighted over-determined scheme, b) Exact three band scheme and c) the best performed scheme (MER_BU_RAN2). The dashed lines show the bounds of $1\mu gl^{-1}$ for chlorophyll *a*, $1mgl^{-1}$ of tripton and 0.1 m^{-1} for CDOM. The points marked with a cross and a triangle had *in situ* samples taken two days and on the day before the satellite overpass respectively, and the points marked with a square had *in situ* samples taken on the day of the satellite overpass.

3.5 August 2009 Validation

Water samples were taken from the surface water at 25 observations stations (shown in Figure 2) on the afternoon of 12th August 2009 between 1:40 pm and 4:10 pm. The image was obtained by the MERIS sensor at approximately 10am the next day.

The MERIS image of the 13th August 2009 was obtained as it was closest in time to the field observations of 12th August 2009. Between the collection of the samples and the satellite overpass no significant inflows were recorded from the source rivers and the site experienced light winds. The MIM algorithm was applied to this image and the water quality parameter concentrations were retrieved. The water quality parameter maps produced from the 13th August 2009 image are shown in Figure 12 and a comparison of the laboratory concentrations and image retrieved concentrations for selected weighting schemes are shown in Figure 13. The means of the absolute values of difference between the laboratory measured concentrations and those retrieved from the image are shown in Table 3.

Table 3 The means of the absolute values of difference between the laboratory measured concentrations and those retrieved from the 13th August 2009 image for selected weighting schemes.

	Chl (μgl^{-1})	
	Av	SD
NO_WEIGHTS	5.96	1.26
3_BANDS	2.81	1.16
MER_BL_RAN1	7.08	1.14
MER_BL_REF3	2.73	1.48
MER_BU_DER6	4.64	2.14
MER_BU_RAN1	0.88	0.61
MER_BU_RAN2	0.78	0.70

The differences displayed by the laboratory-image comparison may not be entirely attributed to errors in the retrieval algorithm. Whilst there were benign weather conditions between the *in situ* sampling and image acquisition, the 18-20 hour time difference is sufficient for the dynamic nature of the water body to be a factor.

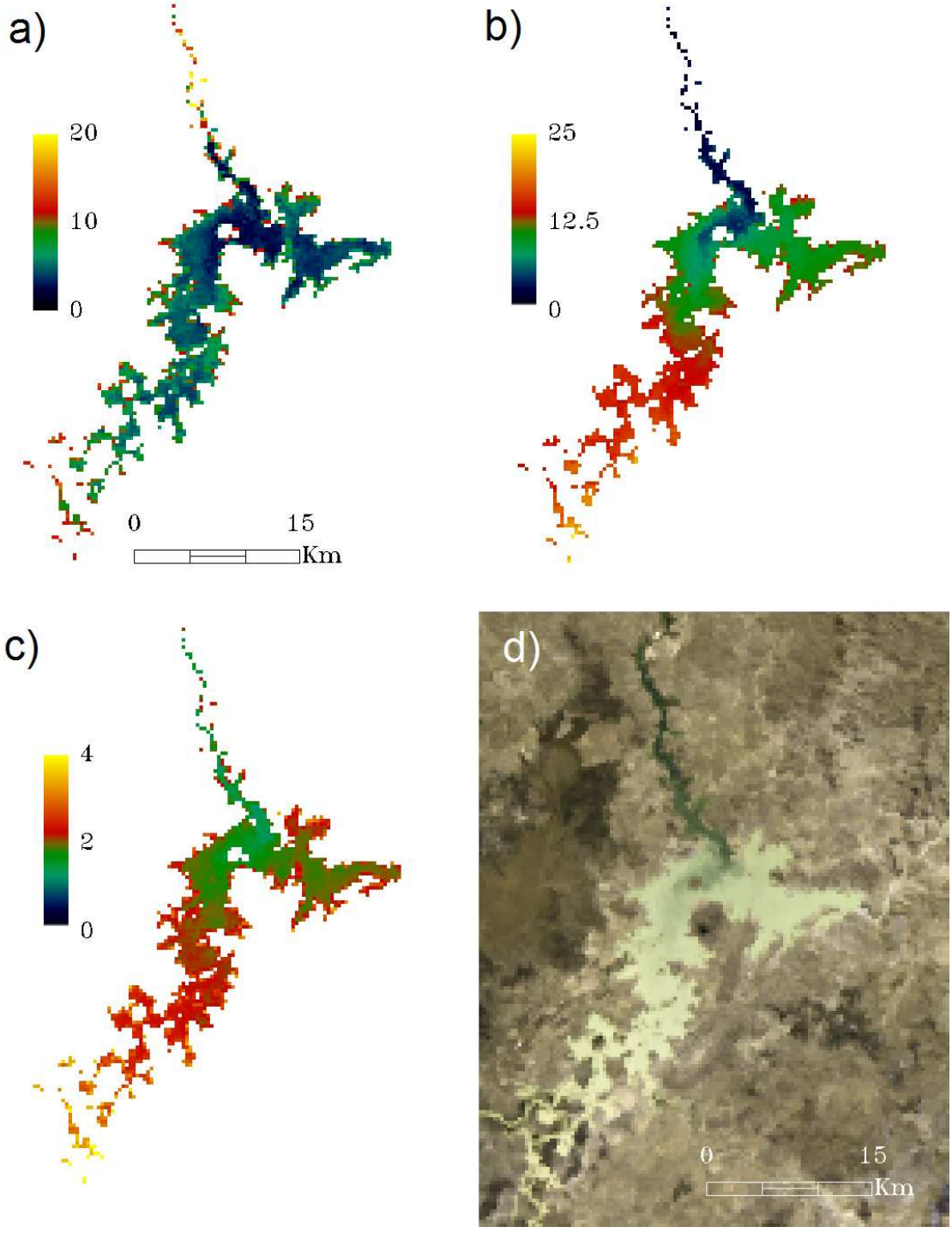

Figure 12 Maps of the water quality parameters retrieved from the 13th August 2009 image using the ratio threshold and the MER_BU_RAN2 weighting scheme. a) Chlorophyll *a,* b) Tripton, c) CDOM and d) True colour MERIS image.

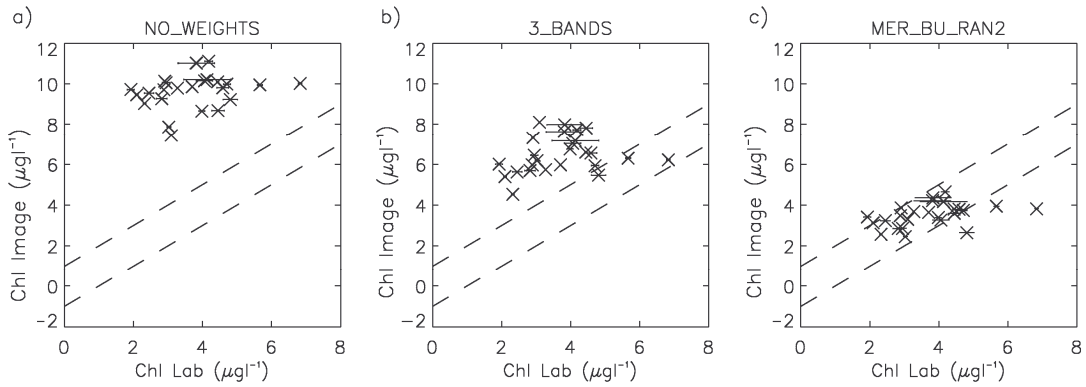

Figure 13 The laboratory concentrations vs. image retrieved concentrations for selected weighting schemes for the 13th August 2009 image, a) Unweighted over-determined scheme, b) Exact three band scheme and c) the best performed scheme (MER_BU_RAN2). The dashed lines show the bounds of 1μgl^{-1} for chlorophyll *a*.

4. Discussion

A comparison between Table 2 and Table 3 shows that the accuracy and precision of the chlorophyll *a* retrieval in the 2009 image is comparable to, if not better than the 2008 image.

There will be uncertainty with any experimental determination of the AOT. The suitability of the atmospheric correction of the 2008 image was confirmed by comparing it to co-incident *in situ* radiometric measurements at three places in the image. To investigate the effect of selecting either of the next reasonable estimates of the AOT, a simple test was performed on the 13th August 2009 image. The image was corrected using AOT at 550nm values higher (0.11) and lower (0.07) than the figure provided by the DDV approach. These images were then inverted using the MER_BU_RAN2 weighting scheme and the change in retrieved concentration was calculated. To isolate the effect of the atmospheric correction, the differences were only calculated on those pixels that selected the same SIOP set in both inversions. In the comparison of 0.07 AOT at 550nm and 0.09 AOT at 550 nm 98.9% of the pixels were used and in the comparison of 0.09 AOT at 550nm and 0.11 AOT at 550 nm 99.6% of the pixels were used.

The chlorophyll *a* retrieval had a mean of -0.028 μgl^{-1} (sd 0.222 μgl^{-1}) for the 0.07-0.09 difference and a mean 0.009 μgl^{-1} (sd 0.270 μgl^{-1}) for the 0.09-0.11 difference. The tripton retrieval had a mean of -0.025 mgl^{-1} (sd 0.120 mgl^{-1}) for the 0.07-0.09 difference and a mean -0.010 mgl^{-1} (sd 0.124 mgl^{-1}) for the 0.09-0.11 difference. In all cases the

distribution of the differences are centred close to zero but it is clear that the tripton is less sensitive to the atmospheric correction as the standard deviation of the differences is smaller in both the under and over corrected cases. The low values of the AOT in this case will reduce the importance of the atmospheric correction. With this is mind and the result of the exercise, it is likely that a poor atmospheric correction will have a greater effect on the chlorophyll *a* rather than tripton determination for Australian water bodies.

In both validation sets the preferred retrieval weighting scheme (MER_BU_RAN2) had a lower mean difference for the chlorophyll *a* estimation than the conventional exact three band or unweighted over-determined system schemes. In the two latter cases chlorophyll *a* was systematically overestimated when compared to the laboratory measurements whereas the weighted scheme neither underestimated nor overestimated. If the two validation sets are pooled the MER_BU_RAN2 weighting scheme has a mean difference of chlorophyll *a* retrieval of 1.0 μgl^{-1}, the three band scheme had a mean difference of 4.2 μgl^{-1} and the unweighted scheme had a mean difference of 5.5 μgl^{-1}. This is not to say that this is the definitive error for the method as a number caveats should be attached to these results. Firstly, the range of water quality parameter concentrations measured in the two field campaigns was limited. For example, the measured *in situ* chlorophyll *a* values ranged from 1.8-7.7 μgl^{-1}, but 80% of the values within the range of 2.7-5.5 μgl^{-1}. The minimum detection limits and retrieval accuracy of water quality parameters are dependent on the parameter as well as the concentrations of the other colour producing agents in the water. Likewise, there is no way to evaluate the accuracy of the atmospheric correction on any particular image without some additional *in situ* data. Lastly, it is not possible to be definitive about the accuracy when there is notable uncertainty in the ground truth values. An attempt to quantify this uncertainty was made which showed the mean difference between the two replicate groups was 0.3 μgl^{-1} (8%) with a standard deviation of 0.35 μgl^{-1} (9%) and the maximum difference was 1.36 μgl^{-1} (33%).

The assessment of the average difference for tripton retrieval suffers from the same caveats as those mentioned from the chlorophyll *a* retrieval: that is, a limited range and

uncertainty in the ground truth data. Unfortunately the tripton concentrations for the 2009 campaign were unable to be determined so only the results for the October 2008 image will be discussed and their usefulness is limited by the sample size of ten. The best performed MER_BL_REF3 weighting scheme had a mean difference of 1.2 mgl^{-1}, the three band scheme had a mean difference of 3.4 mgl^{-1} and the unweighted scheme had a mean difference of 1.8 mgl^{-1}. Although in this case the difference between the weighted and unweighted schemes was not significant at the 95% level it was significant at the 70% level.

As with tripton, the assessment of the CDOM retrieval accuracy suffers from a small sample size but it was found that the best performed MER_BL_RAN1 weighting scheme had a mean difference of 0.12 m^{-1}, the three band scheme had a mean difference of 0.25 m^{-1} and the unweighted scheme had a mean difference of 0.52 m^{-1}. In this case the difference between the weighted and the three band scheme was significant at only the 85% level and the three band and unweighted scheme difference was significant at only the 90% level.

5. Conclusions

This paper described the work done to validate the findings of the previous work in relation to the MIM approach (Campbell and Phinn 2010). The MIM with semi-analytically estimated values for the anisotropic factor of the underwater light distribution was validated against field observations taken at Burdekin Falls Dam in October 2008 and August 2009. The paper then showed how that optical closure can be used to identify the most appropriate SIOP set in water bodies like Burdekin Falls Dam that have multiple SIOP domains. Finally, the laboratory measured water quality parameter concentrations were used to calculate the accuracy and precision of the MIM approach, albeit with a smaller sample size in the case of the tripton concentration retrieval. It was found that significant improvements in the accuracy and precision of retrieved water quality parameter values can be obtained by using differentially weighted, over-determined systems of equations, rather than exact solutions.

A rudimentary test showed that the estimation of water quality parameter concentrations was only slightly affected by errors in the atmospheric correction for this study site. The simulation in Campbell & Phinn (2010) showed that the difference had a linear response to an increase in atmospheric noise and the test in this chapter showed that the gradient of the line was reasonably flat for a practical application. This result is encouraging as it suggests that the risks inherent in the approximations and assumptions in the atmospheric correction may be reasonable for Australian water bodies.

Acknowledgements

The authors would like to thank the CSIRO Water for a Healthy Country Flagship for supporting the field work and the laboratory work . In particular we would like to thank Mr Paul Daniel for his assistance in the field operations, Lesley Clementson of CMAR for the 2008 laboratory measurements and Britta Schaffelke and Michele Skuza of the Australian Institute of Marine Science in Townsville for the 2009 chlorophyll *a* measurements. We would like to thank the European Space Agency for providing the MERIS FR images under the AO 595 agreement. We would like to express our gratitude to the water body operators Sunwater for their assistance in the field operations.

References

Acharya, P.K., Berk, A., Anderson, G.P., Larsen, N.F., Tsay, S.C., & Stamnes, K.H. (1999), 'MODTRAN4: Multiple scattering and bi-directional reflectance distribution function (BRDF) upgrades to MODTRAN', in A.M. Larar (ed.), *Proc. of SPIE, Optical Spectroscopy Techniques and Instrumentation for Atmospheric and Space Research III*, vol. 3756, pp. 354-362.

Adler-Golden, S., Berk, A., Bernstein, L.S., Richtsmeier, S., Acharya, P.K., Matthew, M.W., Anderson, G.P., Allred, C.L., Jeong, L.S., & Chetwynd, J.H. (1998), 'A Modtran4 Atmospheric Correction Package for Hyperspectral Data', in *In Proceedings of AVIRIS Airborne Geoscience Workshop*, Pasadena, CA.

Arar, E.J., & Collins, G.B. (1997). *Method 445.0, In Vitro Determination of Chlorophyll a and Pheophytin a in Marine and Freshwater Algae by Fluorescence, Revision 1.2.* Cincinnati, OH: National Exposure Research Laboratory, Office of Research and Development, U.S. Environmental Protection Agency

Bagheri, S., Peters, S., & Yu, T. (2005). Retrieval of marine water constituents from AVIRIS data in the Hudson/Raritan Estuary. *International Journal of Remote Sensing, 26*, 4013 - 4027

Bainbridge, Z., Brodie, J., Lewis, S., Duncan, I., Post, D., Faithful, J., & Furnas, M. (2006a). Event-based water quality monitoring in the Burdekin Dry Tropics Region: 2004/05 wet season. ACTFR Report No. 06/01 for the Burdekin Dry Tropics NRM. (p. 83). Australian Centre for Tropical Freshwater Research, James Cook University, Townsville.,

Bainbridge, Z., Lewis, S., Brodie, J., Faithful, J., Maughan, M., Post, D., O'Reagain, P., Bartley, R., Ross, S., Schaffelke, B., McShane, T., & Baynes, L. (2006b). Monitoring of sediments and nutrients in the Burdekin Dry Tropics Region: 2005/06 wet season. ACTFR Report No. 06/13 for the Burdekin Dry Tropics NRM. (p. 97). Centre for Tropical Freshwater Research, James Cook University, Townsville.,

Baruah, P.J., Tamura, M., Oki, K., & Nishimura, H. (2001), 'Neural network modeling of lake surface chlorophyll and suspended sediment from Landsat TM imagery', in *22nd Asian Conference of Remote Sensing*, Singapore, pp. 911-916.

Boss, E., & Roesler, C.S. (2006). Over Constrained Linear Matrix Inversion with Statistical Selection. In Z. Lee (Ed.), *Report of the International Ocean-Colour Coordinating Group No. 5: Remote Sensing of Inherent Optical Properties: Fundamentals, Tests of Algorithms, and Applications* Dartmouth, Canada: International Ocean-Colour Coordinating Group

Brando, V.E., & Dekker, A.G. (2003). Satellite hyperspectral remote sensing for estimating estuarine and coastal water quality. *IEEE Transactions on Geoscience and Remote Sensing, 41*, 1378-1387

Campbell, G., & Phinn, S.R. (2010). An assessment of the accuracy and precision of water quality parameters retrieved with the Matrix Inversion Method. *Limnology and Oceanography Methods, 8*, 16-29

Campbell, G., Phinn, S.R., & Daniel, P. (2011). The specific inherent optical properties of three sub-tropical and tropical water reservoirs in Queensland, Australia. *Hydrobiologia, 658*, 233-252

Candiani, G., Giardino, C., & Brando, V.E. (2007a), 'Adjacency Effects and Bio-Optical Model Regionalisation: MERIS Data to Assess Lake Water Quality in the Subalpine Ecoregion ', in H. Lacoste, & L. Ouwehand (eds), *Envisat Symposium 2007*, Montreux, Switzerland.

Candiani, G., Giardino, C., Brando, V.E., Bartoli, M., & Reverberi, F. (2007b). MERIS timeseries data to detect water quality in Subalpine lakes. In, *3rd Workshop Remote Sensing of the Coastal Zone*. Bolzano, Italy

CEOS, (2008). CEOS recommended solar irradiance spectrum for use in Earth Observation applications.[available on internet at http://eocalibration.wordpress.com/2006/12/15/ceos-recommended-solar-irradiance-spectrum-for-use-in-earth-observation-applications, accessed 3 September, 2008]

Commonwealth Bureau of Meteorology, (2010). Climate statistics for Australian locations.[available on internet at http://www.bom.gov.au/climate/averages/tables/cw_034002.shtml, accessed 25th November 2010]

de Haan, J.F., Kokke, J.M.M., Dekker, A.G., & Rijkeboer, M. (1999). *Remote sensing algorithm development, TOOLKIT for water quality continued. Operationalisation of tools for the analysis and processing of remote sensing data of coastal and inland waters. National Remote Sensing Program (NRSP) report-98-12*. Beleids Comissie Remote Sensing (Dutch Remote Sensing Board)

Doerffer, R., & Schiller, H. (2007). The MERIS Case 2 water algorithm. *International Journal of Remote Sensing, 28*, 517 - 535

Doerffer, R., & Schiller, H. (2008). Algorithm Theoretical Basis Document (ATBD) MERIS Regional Coastal and Lake Case 2 Water Project Atmospheric Correction ATBD. GKSS Forschungszentrum, Geesthacht

ESA, (2006). MERIS Product Handbook Ver 2.1.[available on internet at http://envisat.esa.int/pub/ESA_DOC/ENVISAT/MERIS/meris.ProductHandbook.2_1.pdf , accessed 19 April 2009]

Floricioiu, D., & Rott, H. (2005), 'Atmospheric Correction of MERIS Data Over Perialpine Regions', in *MERIS (A)ATSR Workshop 2005 (ESA SP-597).* Frascati, Italy.

Giardino, C., Brando, V.E., Dekker, A.G., Strombeck, N., & Candiani, G. (2007). Assessment of water quality in Lake Garda (Italy) using Hyperion. *Remote Sensing of Environment, 109*, 183-195

Gordon, H.R., Brown, O.B., & Jacobs, M.M. (1975). Computed relationships between the inherent and apparent optical properties of a flat homogeneous ocean. *Applied Optics, 14*, 417-427

Guanter, L., Ruiz-Verdú, A., Odermatt, D., Giardino, C., Simis, S., Estellés, V., Heege, T., Domínguez-Gómez, J.A., & Moreno, J. (2010). Atmospheric correction of ENVISAT/MERIS data over inland waters: Validation for European lakes. *Remote Sensing of Environment, 114*, 467-480

Hakvoort, H., de Haan, J.F., Jordans, R.R.W., Vos, R.J., Peters, S.W.M., & Rijkeboer, M. (2002). Towards airborne remote sensing of water quality in The Netherlands--validation and error analysis. *ISPRS Journal of Photogrammetry and Remote Sensing, 57*, 171-183

Hoge, F.E., & Lyon, P.E. (1996). Satellite retrieval of inherent optical properties by linear matrix inversion of oceanic radiance models: An analysis of model and radiance measurement errors. *Journal of Geophysical Research, 101*, 16631-16648

Hoge, F.E., Wright, C.W., Lyon, P.E., Swift, R.N., & Yungel, J.K. (1999). Satellite Retrieval of the Absorption Coefficient of Phytoplankton Phycoerythrin Pigment: Theory and Feasibility Status. *Applied Optics, 38*, 7431-7441

Hoogenboom, H.J., Dekker, A.G., & Althuis, I.A. (1998a). Simulation of AVIRIS sensitivity for detecting chlorophyll over coastal and inland waters. *Remote Sensing of Environment, 65*, 333-340

Hoogenboom, H.J., Dekker, A.G., & de Haan, J.F. (1998b). Retrieval of chlorophyll and suspended matter from imaging spectrometry data by matrix inversion. *Canadian Journal of Remote Sensing, 24*, 144-152

Kaufman, Y.J., & Tanre, D. (1992). Atmospherically resistant vegetation index (ARVI) for EOS-MODIS. *Geoscience and Remote Sensing, IEEE Transactions on, 30*, 261-270

Keller, P.A. (2001a). Comparison of two inversion techniques of a semi-analytical model for the determination of lake water constituents using imaging spectrometry data. *The Science of The Total Environment, 268*, 189-196

Keller, P.A. (2001b) Imaging spectroscopy of lake water quality parameters., PhD thesis, Remote Sensing Series 36, Remote Sensing Laboratories, University of Zurich.

Kishino, M., Takahashi, M., Okami, N., & Ichimura, S. (1985). Estimation of the spectral absorption coefficients of phytoplankton in the sea. *Bulletin of Marine Science, 37*, 634-642

Kotchenova, S.Y., Vermote, E.F., Levy, R., & Lyapustin, A. (2008). Radiative transfer codes for atmospheric correction and aerosol retrieval: intercomparison study. *Applied Optics, 47*, 2215-2226

Lee, Z., Carder, K.L., & Arnone, R.A. (2002). Deriving Inherent Optical Properties from Water Color: a Multiband Quasi-Analytical Algorithm for Optically Deep Waters. *Applied Optics, 41*, 5755-5772

Leroy, M., Bruniquel-Pinel, V., Hautecoeur, O., Bréon, F.M., & Baret, F. (1998). Corrections atmosphériques des données MERIS/ENVISAT: caractérisations de la BRDF de surfaces “sombres” (p. 98). European Space Agency final report,

Lewis, S.E., Bainbridge, Z.T., Sherman, B.S., Brodie, J.E., & Cooper, M. (2009). The trapping efficiency of the Burdekin Falls Dam: Estimates from a three-year monitoring program. (p. 31). Marine and Tropical Sciences Research Facility. Reef and Rainforest Research Centre Limited and Australian Centre for Tropical Freshwater Research (ACTFR), Townsville

Lyon, P.E., & Hoge, F.E. (2006). The Linear Matrix Inversion Algorithm. In Z. Lee (Ed.), *Report of the International Ocean-Colour Coordinating Group No. 5: Remote Sensing of Inherent Optical Properties: Fundamentals, Tests of Algorithms, and Applications* Dartmouth, Canada: International Ocean-Colour Coordinating Group

Maffione, R.A., & Dana, D.R. (1997). Instruments and methods for measuring the backward-scattering coefficient of ocean waters. *Applied Optics, 36*, 6057-6067

Maritorena, S., Siegel, D.A., & Peterson, A.R. (2002). Optimization of a semianalytical ocean color model for global-scale applications. *Applied Optics, 41*, 2705-2714

Matarrese, R., Chiaradia, M.T., De Pasquale, V., & Pasquariello, G. (2004), 'Chlorophyll-a concentration measure in coastal waters using MERIS and MODIS data', in *IGARSS 2004: IEEE International Geoscience and Remote Sensing Symposium Proceedings, Vols 1-7 - Science for Society: Exploring and Managing a Changing Planet*, vol. 6, pp. 3639-3641.

Mobley, C.D., Sundman, L., Davis, C.O., Bowles, J.H., Downes, T.V., Leathers, R.A., Montes, M.J., Bissett, W.P., Kohler, D.D.R., Reid, R.P., Louchard, E.M., & Gleason, A. (2005). Interpretation of hyperspectral remote-sensing imagery by spectrum matching and look-up tables. *Applied Optics, 44*, 3576-3592

Moore, G.F., Aiken, J., & Lavender, S.J. (1999). The atmospheric correction of water colour and the quantitative retrieval of suspended particulate matter in Case II waters: application to MERIS. *International Journal of Remote Sensing, 20*, 1713-1733

Morel, A. (1974). Optical properties of pure water and pure seawater. In N.G. Jerlov, & E. Steeman Nielsen (Eds.), *Optical Aspects of Oceanography* (pp. 1-24). London: Academic Press Inc

O'Reagain, P.J., Brodie, J., Fraser, G., Bushell, J.J., Holloway, C.H., Faithful, J.W., & Haynes, D. (2005). Nutrient loss and water quality under extensive grazing in the upper Burdekin river catchment, North Queensland. *Marine Pollution Bulletin, 51*, 37-50

O'Reilly, J.E., Maritorena, S., Mitchell, B.G., Siegel, D.A., Carder, K.L., Garver, S.A., Kahru, M., & McClain, C. (1998). Ocean color chlorophyll algorithms for SeaWiFS. *Journal of Geophysical Research, 103*, 24937-24953

Odermatt, D., Giardino, C., & Heege, T. (2010). Chlorophyll retrieval with MERIS Case-2-Regional in perialpine lakes. *Remote Sensing of Environment, 114*, 607-617

Phinn, S.R., Roelfsema, C., Scarth, P., Dekker, A.G., Brando, V.E., Anstee, J.M., & Marks, A. (2005). An integrated remote sensing approach for adaptive management of complex coastal waters. Final Report - Moreton Bay Remote Sensing Tasks (MR2), CRC for Coastal Zone, Estuary & Waterway Management., *Estuary & Waterway Management, Indooroopilly.* CRC for Coastal Zone, Brisbane

Pope, R.M., & Fry, E.S. (1997). Absorption spectrum (380 -700 nm) of pure water. II. Integrating cavity measurements. *Applied Optics, 36*, 8710-8723

Rijkeboer, M., Dekker, A.G., & Gons, H.J. (1997). Subsurface irradiance reflectance spectra of inland waters differing in morphometry and hydrology. *Aquatic Ecology, 31*, 313-323

Santer, R., Carrere, V., Dessailly, D., Dubuisson, P., & Roger, C., (2006). Algorithm theoretical basis document (ATBD) 2.15: Atmospheric corrections over land.,[available on internet at http://envisat.esa.int/instruments/meris/pdf/atbd_2_15.pdf, accessed 24 November 2006]

Santer, R., Carrere, V., Dubuisson, P., & Roger, J.C. (1999). Atmospheric correction over land for MERIS. *International Journal of Remote Sensing, 20*, 1819-1840

Santini, F., Alberotanza, L., Cavalli, R.M., & Pignatti, S. (2010). A two-step optimization procedure for assessing water constituent concentrations by hyperspectral remote sensing techniques: An application to the highly turbid Venice lagoon waters. *Remote Sensing of Environment, 114*, 887-898

Schaale, M., Fischer, J., & C. Olbert (1998), 'Quantitative estimation of substances contained in inland water from multispectral airborne measurements by neural networks', in *ASPRS-RTI Annual Conference*, Tampa, USA, pp. 1345-1356.

Smith, R.C., & Baker, K.S. (1981). Optical properties of the clearest natural waters (200-800 nm). *Applied Optics, 20*, 177-184

Sterckx, S., & Debruyn, W. (2004), 'A hyperspectral view of the North Sea', in *Proceedings of the Airborne Imaging Spectroscopy Workshop* Bruges, p. 9.

Su, F.C., Ho, C.R., Zheng, Q., Kuo, N.J., & Chen, C.T. (2006). Satellite chlorophyll retrievals with a bipartite artificial neural network model. *International Journal of Remote Sensing, 27*, 1563-1579

Thuillier, G., Hersé, M., Labs, D., Foujols, T., Peetermans, W., Gillotay, D., Simon, P.C., & Mandel, H. (2003). The solar spectral irradiance from 200 to 2400 nm as measured by the SOLSPEC spectrometer from the Atlas and Eureca missions. *Solar Physics, 214*, 1-22

Tilstone, G.H., Moore, G.F., Sorensen, K., Doerffer, R., Rottgers, R., Ruddick, K.G., Pasterkamp, R., & Jorgensen, P.V. (2002). *REVAMP protocols document*. European Space Agency

Van Heukelem, L., & Thomas, C.S. (2001). Computer-assisted high-performance liquid chromatography method development with applications to the isolation and analysis of phytoplankton pigments. *Journal of Chromatography A, 910*, 31-49

Vermote, E.F., Tanré, D., Deuzé, J.L., Herman, M., Morcrette, J.J., Kotchenova, S.Y., & Miura, T., (2006). Second simulation of the satellite signal in the solar spectrum (6S), 6S user guide version 3.[available on internet at http://6s.ltdri.org/6S_code2_thiner_stuff/6s_ltdri_org_manual.htm accessed 11 August 2008]

Vidot, J., & Santer, R. (2005). Atmospheric correction for inland waters - application to SeaWiFS. *International Journal of Remote Sensing, 26*, 3663-3682

Vos, R.J., Hakvoort, J.H.M., Jordans, R.R.W., & Ibelings, B.W. (2003). Multiplatform optical monitoring of eutrophication in temporally and spatially variable lakes. *The Science of The Total Environment, 312*, 221-243